Liquid identification by using a micro-electro-mechanical interdigital transducer

Bui, Thu Hang; Morana, Bruno; Akhnoukh, Atef; Chu Duc, Trinh ; Sarro, Pasqualina M.

DOI
10.1039/c6an01804a

Publication date
2017

Document Version
Accepted author manuscript

Published in
The Analyst

Accepted Author Manuscript of http://dx.doi.org/10.1039/c6an01804a

Liquid Identification by a Micro-electro-mechanical Interdigital Transducer

ThuHang Bui,[1, 2 a)] Bruno Morana,[1)] Atef Akhnoukh,[1)] Trinh Chu Duc,[2)] and Pasqualina M. Sarro[1)]

[1]*Microelectronics, Delft University of Technology, Delft, 2628 BX, The Netherlands*

[2]*Electronics and Telecommunications, University of Engineering and Technology, VNU-HN, Hanoi, Vietnam*

A surface-acoustic-mode Aluminum Nitride (AlN) transducer is utilized to determine the type of liquid dropped on the propagation path. It is based on tracking the shrinking droplet radius and observing stagnant liquid molecules during and after the liquid evaporation process. The device configuration is suitable to test small amounts of liquids, in the microliter range. According to both mass loading and physical property mechanisms, eight samples of liquids, isopropanol (IPA), ethanol (ETH), deionized-water (DW), tap water (TW), heptane (HEP), propylene glycol monomethyl ether acetate (PGMEA), hexamethyldisilazane (HMDS) and acetone (ACE), which have different equilibrium vapor pressures, molecular weights and boiling points, are accurately detected. The experimental results show that the rate of the change in the energy loss including a slow and fast attenuation region depends on the change of physical properties, such as density, sound speed in liquids and evaporation rate, during the evaporation process. As the evaporation rate of the DW is rather slow, the slow attenuation region occurs for a longer time than the fast one. Consequently, the whole oscillation duration of the attenuation occurs for a longer time, whereas that of the other liquids studied, like ACE, ETH, IPA having a faster evaporation rate is shorter. Sensitivities of the surface-acoustic-mode transducer to the evaporate process of liquids such as DW, TW, PGMEA, HMDS, HEP, IPA, ETH and ACE are -29.39, -29.53, -31,79, -34.12, -33.62, -32.87, -32.67, -32.82 dB/μm^2. The concentration of stagnant liquid molecules causes a change in the surface mass of the micro-electro-mechanical transducer, which causes a frequency shift and increases signal noise at the receiver after the liquid evaporation process. The average frequency shifts of ACE, HEP, HMDS, ETH, IPA, PGMEA, TW and DW are 241, 206, 172, 117, 76, 27.3, 11.6 and 0 kHz, respectively, coherent with the type of formed liquid patterns on the device surface, thus allowing to detect liquid samples effectively.

[a] Author to whom correspondence should be addressed. Email: t.h.bui@tudelft.nl.
Contributed paper, published as part of the Proceedings of the 14th IEEE Sensors, South Korea, Nov. 2015.

I. INTRODUCTION

An interdigital transducer generates several acoustic wave modes. Shear horizontal acoustic plate mode (SH-APM), shear horizontal surface acoustic wave (SH-SAW) mode, love wave and flexural plate wave (FPW) mode, have been utilized for many microfluidic applications[1-4] whereas a surface acoustic wave (SAW) mode is very appealing for gas sensing applications due to the sensitivity to surface perturbations induced by pressure or mass loading[5]. Owing to the leakage phenomenon of a longitudinal wave component into a liquid medium, the SAW device is rarely used in liquid sensing applications where generally a large liquid volume is placed on the whole propagation path[5-6]. However, this component is extremely sensitive to surface mass density induced by the active force of an object, such as a thin gold film[7], a microliter droplet[8], a moving liquid[9-11], and contaminated liquid[12] on or through the piezoelectric surface. For liquid applications, a measurable energy loss detects the type of liquid. In our previous work, identification of the liquid present on the propagation path is based on stagnant liquid molecules on the surface[8]. In this paper, we employ physical properties, such as the liquid evaporation rate, sound speed and density, to enhance the accuracy of surface-acoustic-mode Aluminum Nitride (AlN) transducers.

In all commonly used biosensors for microfluidic applications, such as interdigital sensors (SH-SAW, SH-APM and FPW mode[5]), transducer resonators[13] and capacitive sensors[14-15], detection mechanisms are based on one property like mass loading (a frequency change can result from an absorption of the contacting liquid without the attenuation effects)[16], physical properties (changes in operating frequency and attenuation effects induced by rheological properties or thermal effects of any liquid medium in contact with the piezoelectric)[16, 17], resistance and capacitance properties (changes induced by the dielectric constant of the medium between the plates or fluidic pressure variation)[14, 15]. We employ both physical properties (liquid density, sound speed in liquids and evaporation rate) and mass loading (concentration of stagnant liquid molecules) during and after the evaporation process to identify the liquid. Specifically, during this process, a phase transition from liquid to gas phase of the molecules at the droplet surface takes place quickly or slowly depending on the evaporation rate of each liquid[18]. It leads to a different attenuation duration for SAWs for each liquid. This attenuation variation depends on the density and sound speed in liquids. When the dynamic equilibrium is reached, the evaporation process stops. There are liquid molecules left on the surface, which alter the mass density of the piezoelectric surface. Taking advantage of these distinct physical properties, we have developed a potential method to identify the type of liquid being studied. This novel method uses a SAW transducer with a large IDT aperture and with a cavity to accommodate small volumes (µl range) of liquids. The oscillation variation and duration in the magnitude of the insertion loss during the evaporation process are analyzed and experimentally recorded. The evaluation of the relation between surface mass loading of the SAW device and stagnant liquid molecules is described. These are validated by experimental results obtained with eight liquids. The chosen substances include liquids that have similar physical properties

(evaporation rate and density), such as isopropanol (IPA), ethanol (ETH) and acetone (ACE), as well as with quite different properties (evaporation rate, density, sound speed or chemical bond), like deionized -water (DW), tap water (TW), hexamethyldisilazane (HMDS), heptane (HEP) and propylene glycol monomethyl ether acetate (PGMEA).

II. ANALYSIS OF THE TRANSDUCER RESPONSE DURING THE LIQUID EVAPORATION PROCESS

A. The shape of the droplet and the energy attenuation of the SAW device

After the liquid to be identified is dropped on the propagation path of a SAW transducer, the evaporation process of the droplet starts. Before the dynamic equilibrium is reached, the droplet radius decreases and creates a 'blank' area on the surface like a non-leaky medium, and there is a signal at the receiver. Consequently, the transducer response is attenuated due to the smaller energy absorption inside the liquid medium. It changes continuously in correspondence of the variation of the 'blank' area on the surface. The rate of this variation depends on the evaporation rate of the liquid. The power dissipation into the liquid medium is a much more remarkable effect than the frequency shift caused by the change in the surface mass density. Therefore, in this section, this frequency shift is ignored during the evaporation process.

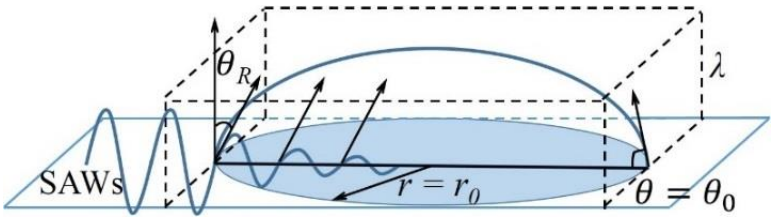

Fig. 1: Schematic view of the initial droplet inside the cavity.

When SAWs travel through a liquid medium, there are two attenuation types, caused by emission of compressive waves and friction loss of shear waves[19]. However, attenuation by viscous friction is often ignored because it is negligible in comparison with the contribution of the Rayleigh component. If SAWs travel through a piezoelectric layer with a thickness λ and a width r, the energy of Rayleigh waves is given by [19]:

$$E = 2\pi^2(\lambda 2r_0)\rho v_R^3 \left(\frac{a}{\lambda}\right)^2 \quad (1)$$

where v_R, a, λ and ρ are the Rayleigh velocity, the amplitude of Rayleigh component, the wavelength and the piezoelectric density, respectively, while r_0 is the droplet radius after dropping the liquid as shown in Fig. 1.

At the contact area between the piezoelectric and the liquid medium, the amplitude of Rayleigh waves is equal to that of longitudinal waves into liquid at Rayleigh angle $\theta_R = acrsin(v_f/v_R) = 17.3^0$, which is assumed to be smaller than the critical

angle θ_0 during the transient evaporation time of the droplet. The volume variation here relates to the shrinking contact radius and the contact angle at a much slower rate, called as constant contact angle (CA)[20]. For the CA mode, the constant contact angle and the height of the droplet are not considered. As the contour of the droplet on the surface is a new circle with variable radius *r*, the energy absorbed into the liquid medium per second is estimated as follows:

$$dE = 2\pi^2(\pi r^2)\rho_f v_f v_R^2 \left(\frac{a}{\lambda}\right)^2 \tag{2}$$

Here, ρ_f and v_f are the liquid density and the liquid velocity, respectively. When the constant contact angle and the height of the droplet are neglected, the fractional change in the total energy loss E_t before and after traveling through the liquid medium is proportional to the fractional change between Rayleigh wave energy losses *E* and *dE* resulting from the leakage of Rayleigh waves into the liquid medium. It is also referred to a proportional coefficient of the energy loss $\alpha(r)$ given by:

$$\alpha(r) = \frac{dE_t}{E_t} \sim \frac{dE}{E} = \frac{1}{2}\pi \frac{r^2}{\lambda r_0} \frac{\rho_f v_f}{\rho v_R} \tag{3}$$

As the contact angle at $\theta_0 = \pi/3$ is assumed to be almost constant and always larger than the Rayleigh angle, the change in droplet radius is in response to the energy loss during the evaporation process. With each liquid, the initial contact angle is different and measured by the video-based optical contact angle measuring instrument. The droplet radius is a function of the time as given by[20, 21]:

$$r^2 = r_0^2 - \frac{2D(c_s - c_\infty)}{\rho_f} g(\theta_0) f(\theta_0) t \tag{4}$$

where $r_0 = \left(\frac{3}{\pi} V_0 \frac{(1+cos\theta_0)^2}{sin\theta_0(2+cos\theta_0)}\right)^{1/3}$, $g(\theta_0) = \frac{sin^3(\theta_0)}{(1-cos\theta_0)^2(2+cos\theta_0)}$ and $f(\theta_0) = \frac{sin\theta_0}{1+cos\theta_0} + 4\int_0^\infty \frac{1+\cosh(2\theta_0\tau)}{\sinh(2\pi\tau)} \tanh[(\pi-\theta_0)\tau] d\tau$.

θ_0, r_0, V_0 are the initial contact angle, the radius and the volume of the droplet, respectively. The diffusion coefficient of the vapor in the atmosphere *D*, the vapor concentration in the saturation atmosphere c_s and at infinity $c_\infty \approx Hc_s$, are different for different liquids and sensitive to the ambient temperature and humidity *H* during the evaporation time. For example, values of some liquids in air at a temperature of 20^0C are shown in Table 1[22, 23, 25].

Table 1: DIFFUSIVITY AND VAPOR CONCENTRATION OF LIQUIDS IN AIR

Liquid	***D*** ***(10^{-6} m^2/s)***	***c_s*** ***(kg/m^3)***
Water	24.46	0.017
Heptane	7.06	0.0941
Ethanol	12.68	0.0375
Acetone	12.12	0.0522

From Eqs. 3 and 4, the fractional change depends on physical properties of the liquid such as density, sound speed in the liquid and rate of evaporation. The fractional change of the CA mode in Fig. 2 is a function of the liquid contact radius related to the initial contact angle $\theta_0 = \pi/3$ and to the liquid volume. It has two descending parts during the transient evaporation time. One refers to a fast attenuation region when the fractional change descends quickly and the other is a slow attenuation region when it varies more slowly. These regions are separated by two tangents of the fractional change line, with a factor 10 difference in slope.

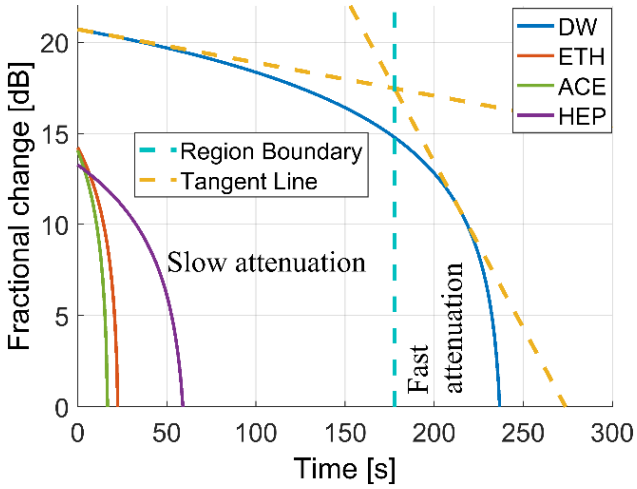

Fig. 2: The dependence of the fractional change on the evaporation time of some liquids for an initial volume of 0.05 µl.

B. Mass sensitivity of the SAW device

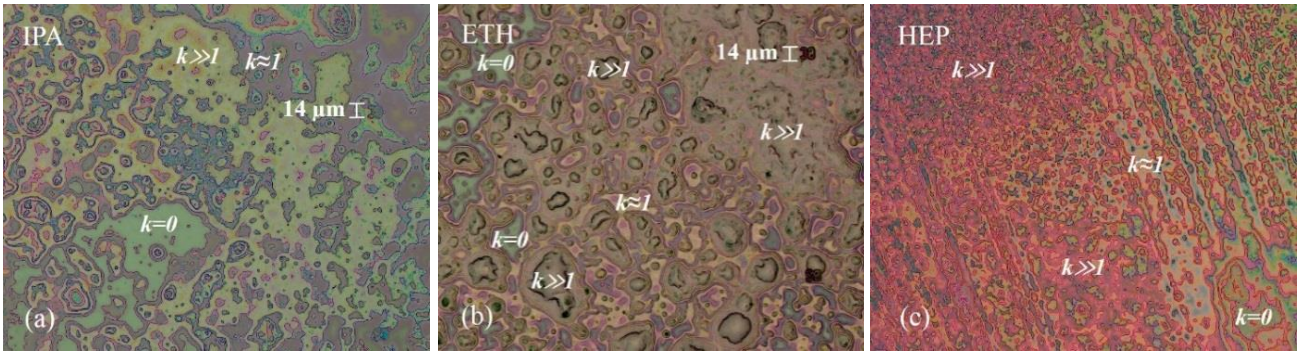

Fig. 3: The pattern formation for (a) IPA, (b) ETH and (c) HEP after the evaporation process.

The second detection mechanism employs a comparison of the variation of the transducer response due to the change in the density mass on the surface. When it reaches the equilibrium, there is no change in the amount of liquid or vapor. Ultimately, as liquid molecules are left after the evaporation process, a change in the surface mass density of the piezoelectric surface is observed. Each liquid has a different pattern formation by the self-assembly of the molecules at the end of the evaporation process. For example, when they have rather different properties like the case for IPA or ETH with HEP, or even when the

physical properties such as the boiling point, the vapor pressure, and the molecular weight are quite similar (IPA and ETH), the concentration and pattern formation of the stagnant liquid molecules are dissimilar (see Fig. 3). At the dynamic equilibrium, the measured transducer responses are almost constant. The fractional change $\alpha(r)$ is approximately zero because the radius of the liquid droplet and the contact angle of the concentrated liquid molecules go to zero (see Eq. 4). Therefore, the absorption caused by the leakage phenomenon is ignored. The remaining liquid molecules after the evaporation form dense monolayers or multilayers k_i of molecules[25] which are also referred as clusters. This leads to perturbations on the surface and change the areal mass density. As chosen liquids are pure and are tested in the same condition, this change only depends on the size (molecular weight) and concentration of the molecules. The stagnant liquid molecules on the solid surface refer to hard macromolecules adhering to the thin AlN film, which cause a roughness increase of the film surface. Regarding the formation of the liquid molecule layers on the thin film, the surface mass density, also called areal density, is given by the ratio of the mass to the area. The area includes the AlN surface a_{AlN} which is not covered by the liquid and total meniscus areas a_l of n liquid clusters. The height of the monolayer cluster meniscus is negligible and the meniscus area is approximated to its 2D projection on the thin film surface. Hence, the average areal density is written by:

$$\rho_s = \frac{m_{AlN}+\sum_{i=1}^{n} m_i}{a_{AlN}+a_l} \approx \begin{cases} \frac{m_{AlN}+\sum_{i=1}^{n} m_i}{a_s} & when\ k_i \approx 1\ (monolayer) \\ \frac{m_{AlN}+\sum_{i=1}^{n} m_i}{a_{AlN}+\sum_{i=1}^{n}\frac{m_i}{\rho d k_i}} & when\ k_i \gg 1\ (multilayer) \end{cases} \quad (5)$$

where m_{AlN}, m_i, a_s, d are the mass of the AlN thin film and of the stagnant liquid cluster i^{th}, the surface area of the thin film before dropping liquid and the thickness of a layer, respectively. If there are N_i stagnant molecules in the cluster i^{th}, the cluster mass is given by:

$$m_i = \frac{N_i * M}{6.02*10^{23}} \quad (6)$$

where M is the molecular weight of the liquid and $K = 6.02*10^{23}$ (mol^{-1}) is Avogadro's number. So, the average surface mass density is rewritten as:

$$\rho_s \approx \begin{cases} \frac{\rho_{AlN}*h+\sum_{i=1}^{n}\frac{N_i*M}{K}}{a_s} \approx \frac{\rho_{AlN}hK+NM}{a_s K} & when\ k_i \approx 1 \\ \frac{\rho_{AlN}*h+\sum_{i=1}^{n}\frac{N_i M}{K}}{a_{AlN}+\sum_{i=1}^{n}\frac{N_i M}{K\rho d k_i}} \approx \frac{\rho_{AlN}hK+NM}{a_{AlN}K+\frac{M}{\rho d}\sum_{i=1}^{n}\frac{N_i}{k_i}} \approx \frac{\rho_{AlN}hK+NM}{a_{AlN}K+\frac{nM}{\rho d}\bar{N}} & when\ k_i \gg 1 \end{cases} \quad (7)$$

where ρ_{AlN}, h, N, $\bar{N}$ are the density and the thickness of the thin film, the total stagnant liquid molecules and the average molecule concertation in the layer of the cluster in contact with the thin film, respectively. After the evaporation process, the

variation of the surface mass density leads to the fractional change in the kinetic energy density of SAWs as well as the negative fractional change of the wave velocity and the operating frequency which is given by[16]:

$$\frac{\Delta U}{U_0} = -\frac{\Delta v}{v_0} = \rho_s \frac{v_0}{4P}\left(v_{x0}^2 + v_{y0}^2 + v_{z0}^2\right) = \rho_s S_m f_0 \tag{8}$$

where v_{x0}, v_{x0}, v_{x0} are the unperturbed SAW velocities on the surface along *X*, *Y*, *Z* axis, respectively. And *P*, U_0 are the power density and the peak of the kinetic energy of SAWs on the AlN thin film. The mass sensitivity factor $S_m = \frac{v_0}{4P}\left(v_{x0}^2 + v_{y0}^2 + v_{z0}^2\right)$ only depends on electromechanical properties of the surface material, thus this factor is mostly constant for any liquid. If the remaining liquid molecules on the surface are negligible, like for deionized water, the mass density change is almost constant. Hence, the change in the kinetic energy density only depends on the mass sensitivity factor of the material. On the contrary, if they are rather significant like for IPA, ETH and HEP (see Fig. 3), the output signal of the SAW device is significantly perturbed. By using a network analyzer in the measurement setup, the SAW device is incorporated as a feed-back-loop oscillator; so that, the fractional frequency variation $\frac{\Delta f}{f_0}$ follows the fractional velocity variation $\frac{\Delta v}{v_0}$ [16, 26]. Therefore, from Eqs. 7 and 8, the fractional change of the frequency is calculated as:

$$\frac{d\Delta f}{f_0^2} \approx S_m S_l dN \qquad where\ S_l = \begin{cases} -\frac{M}{a_s K} & when\ k_i \approx 1 \\ -\frac{M}{a_{AlN}K + \frac{nM}{\rho d}\bar{N}} & when\ k_i \gg 1 \end{cases} \tag{9}$$

Here, S_l is the molecule sensitivity factor which depends on the type of liquid. Besides the characteristics of the thin film, the fractional change of the SAW frequency caused by surface perturbations is dependent on the molecular weight, the average molecule concentration in the layer of the cluster, the number of clusters and the density of the liquid. Especially, for the monolayer pattern of the liquid molecules, it depends only on the molecular weight and the total number of molecules on the propagation path.

III. SAW DEVICE FABRICATION AND CHARACTERIZATION

The device used for experiments (see Fig. 4) is based on our previous design[8], but optimized by enlarging the aperture size and implementing a deep cavity for containing very small liquid volumes (down to 0.1 µl). Main device parameters are summarized in Table 2. With this modified configuration, a more precise detection mechanism based on physical properties and mass loading as presented above, can be experimentally validated. The aim of the fabrication of the deep cavity using the SiO_2 thick film (Fig. 4a) is to prevent contact between the measurement probes and the liquid during the measurement process. The measurement system is shown in Fig. 4b. An immediate frequency (IF) bandwidth of 100 Hz is setup to reduce noise

sidebands and residual frequency modulation (FM) when the radio frequency (RF) signal is mixed with local oscillator (LO) signal of a local oscillator in the network analyzer. Simultaneously, the highest power, 5dBm, is applied at the input port, thus the measurement dynamic range is improved[27].

Table 2: PARAMETERS OF THE SAW TRANSDUCER

Parameters	***Value***	***Unit***
Number of the input and output fingers	40x40	
The cavity	2x2.5	mm^2
The aperture of input and output IDTs	2	mm
IDT finger width $d = \Lambda/4$	10	μm
IDT finger height	0.5	μm
The propagation path between input and output IDTs	1000	μm
The theoritical center frequency f_0	125.3	MHz

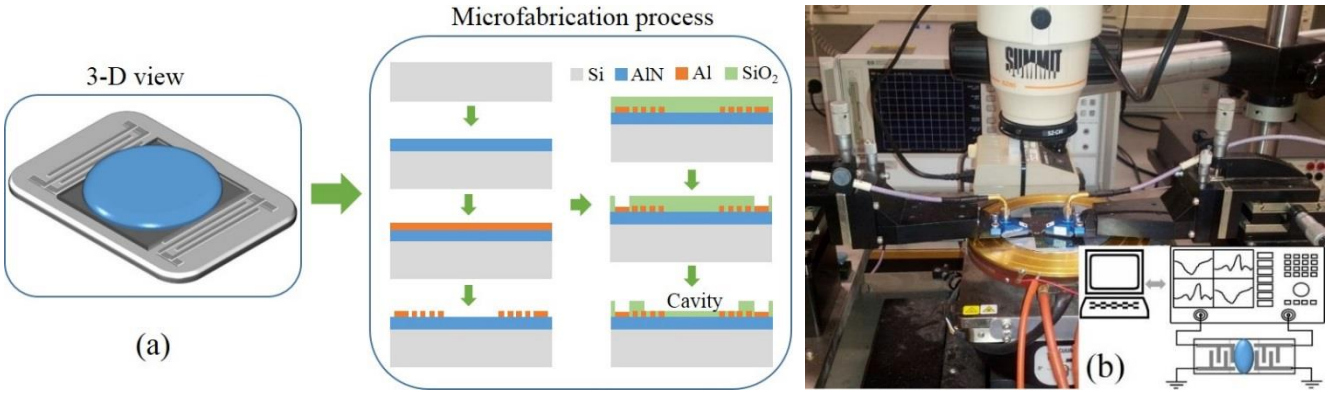

Fig. 4: (a) 3-D view and microfabrication process of the device. (b) The measurement setup of the SAW device for liquid sensing.

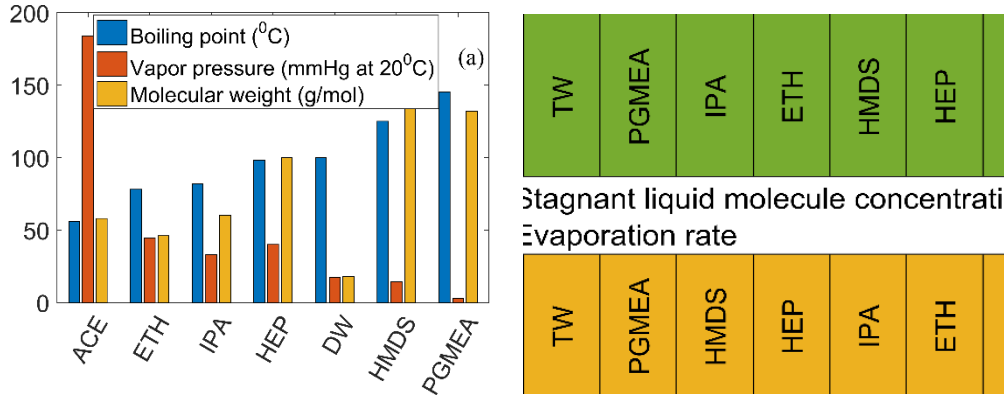

Fig. 5: (a) Physical properties related to the liquid evaporation and (b) the observed order of the increasing liquid evaporation rate and increasing liquid molecule concentration remaining on the surface, consistent with their physical properties.

The evaporation rate of each liquid depends on some physical properties such as boiling point and vapor pressure. In this study, we used eight liquids with different boiling point, vapor pressure and molecule weight, as reported in Fig. 5a. The evaporation rate and the concentration of the stagnant liquid molecules, ordered from low to high, are shown in Fig. 5b. Tap water is quite similar to deionized water but the stagnant molecule concentration is denser and the evaporation rate is estimated

to be quicker because of the presence of mineral ions (sodium iron, copper, bromide and calcium). Water has the slowest evaporation rate because it has a dipole-dipole interactions O-H with the others molecules. Water molecules are interconnected by the hydrogen bonding O-H which is much stronger than the other hydrogen bonding like H-F or C-H. The dipole-dipole interactions O-C for ACE, IPA and HEP are weaker than for water[28]. All tests are executed at the same environment conditions (like temperature, humidity) and initial conditions for each liquid type (like volume). As the surface tension and the cohesive force of some used liquids are weak, they overflow around the cavity after dropping.

IV. RESULTS AND DISCUSSIONS

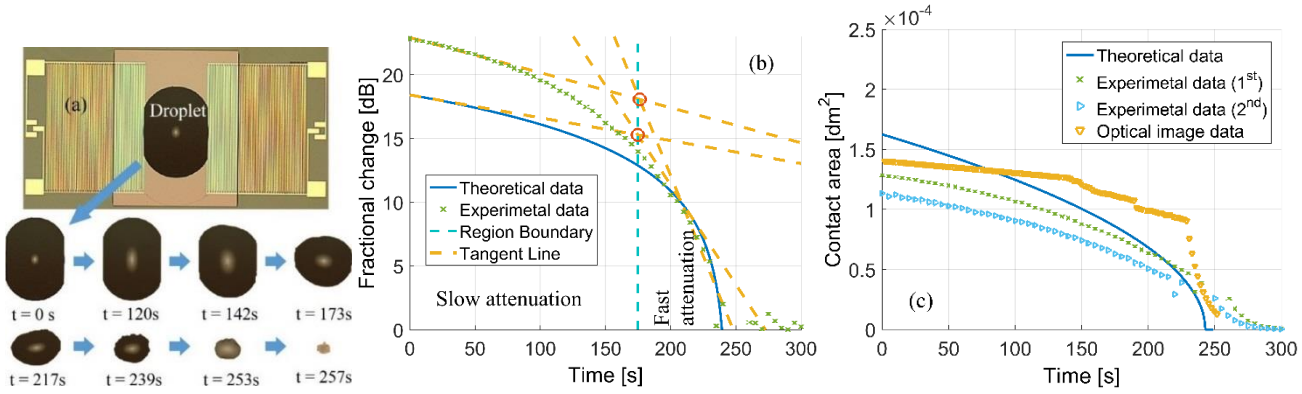

Fig. 6: (a) The evaporation process of a 0.05 µl droplet, at the middle of the SAW propagation path within 257 seconds. (b) Theoretical and experiment data of the fraction changes in insertion loss. (c) Contact area calculated by theoretical, experimental and optical image data.

The optical micrographs of a droplet evaporation process are shown in Fig. 6a. For the first 140 seconds, the slow attenuation region, the droplet shape varies rather slowly and then extremely quickly till it evaporates completely in 257 seconds. At the beginning, the measured insertion loss *IL* has a minor oscillation because of the slight non-uniform energy distribution on the propagation path, the deformation of the contact angle, as well as the slight deformation of the contact radius. Therefore, in fact, there is a gradual movement of the attenuation. The fraction change of the SAW device is calculated by the difference of sequential insertion losses $\alpha(dB) = \Delta IL = \overline{IL_i} - \overline{IL_{i-1}}$. The fractional change varies rather slowly like the change of the droplet shape in the slow attenuation region, as shown in Fig. 6b. When the droplet starts to shrink and changes quickly till it evaporates completely, a fast attenuation occurrence is observed. The duration of these regions depends mostly on contact area deformations of the droplet which is a contact boundary of leaky SAWs from piezoelectric medium to liquid medium. These attenuation regions, in both theoretical and experimental data, are divided by tangent lines with the same factor difference in slope. The region boundary created by a set of tangent lines is a boundary for gradual $d\alpha_1$ and sudden $d\alpha_2$ variation regions of the insertion loss. The comparison of $d\alpha_{1,\,theory}$ = -2.78 x 10^{-1} dB to $d\alpha_{1,\,experiment}$ = -2.61 x10^{-1} dB for the first region and $d\alpha_{2,\,theory}$ = -6.06 x 10^{-1} dB to $d\alpha_{2,\,experiment}$ = -6.75 x 10^{-1} dB for the second region, demonstrates a good match between

theory and experiment. The contact area is calculated by theory, experimental data of the fractional change and optical image as illustrated in Fig. 6c. The Kalman filter method, also called a linear quadratic estimation (LQE), for the object detecting and tracking method is used to calculate contact area of the optical droplet image[29]. The shape of the optical image is a good match compared to the theoretical data and experimental data. Root mean square deviations of the theoretical data with respect to the experimental data are 0.18, 0.3 mm^2. If the sensitivity is defined by $S = d\alpha/da = \frac{1}{2}(\rho_f v_f)/(\lambda r_0 \rho v_R)$, it is -29.39 dB/μm^2. This means that for each 1 μm^2 of the evaporated liquid area, the insertion loss will decrease by 29.39 dB.

This analysis illustrates the fractional change parameter of eight samples in the time domain under the mostly constant ambient conditions as shown in Fig. 7. Observing the variation of the parameter α of eight liquids in the slow and fast attenuation region during the entire evaporation process, we see that water with the slowest evaporation rate has the longest variation of the insertion loss. And slow and fast attenuation regions of water are quite evident. The slow attenuation region of DW, TW, PGMEA, HMDS and HEP appears clearly whereas that of IPA, ETH and ACE disappears. Due to the weak surface tension and cohesive force of liquids such as IPA, ETH, ACE and HEP, the droplet fills the entire propagation path; thus the area contacting the air is larger and makes the evaporation faster. Therefore, the slow attenuation almost disappears and the fast attenuation region is reached quickly. From the fractional change data of each liquid and Eq. 3, the deformation of the contact area can be estimated. For fast attenuation region, average deformation velocities of contact areas are -3.136 x 10^{-10}, -3.269 x 10^{-10}, -3.764 x 10^{-10}, -7.841 x 10^{-10}, -8.731 x 10^{-10}, -1.83 x 10^{-10}, -292 x 10^{-10} and -4.4 x 10^{-10} (m/s)^2 in regards to DW, TW, PGMEA, HMDS, HEP, IPA, ETH and ACE respectively. It is caused by the evaporation rate, density, sound speed and deformation of the droplet shape inside the cavity. Sensitivities of the device to TW, PGMEA, HMDS, HEP, IPA, ETH and ACE are -29.53, -31,79, -34.12, -33.62, -32.87, -32.67, -32.82 dB/μm^2.

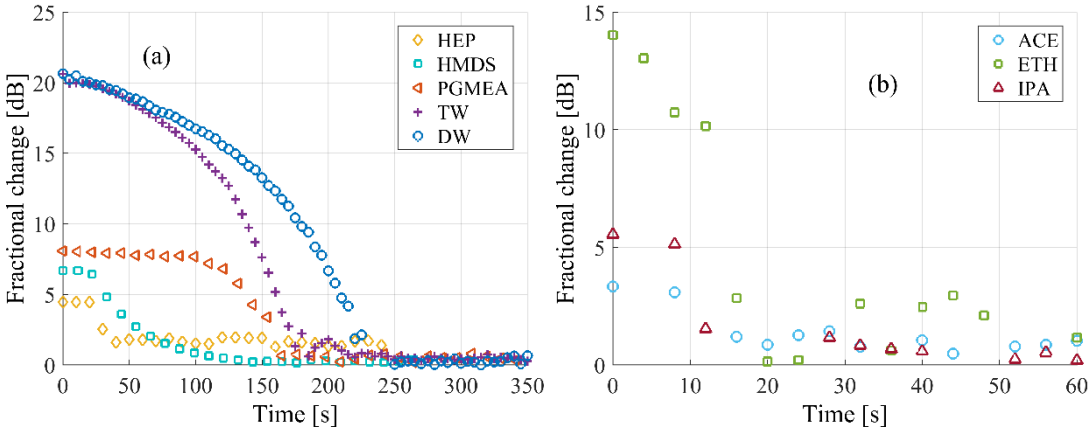

Fig. 7: Fractional change α in insertion loss for (a) HEP, HMDS, PGMEA, TW and DW; and (b) ACE, ETH and IPA.

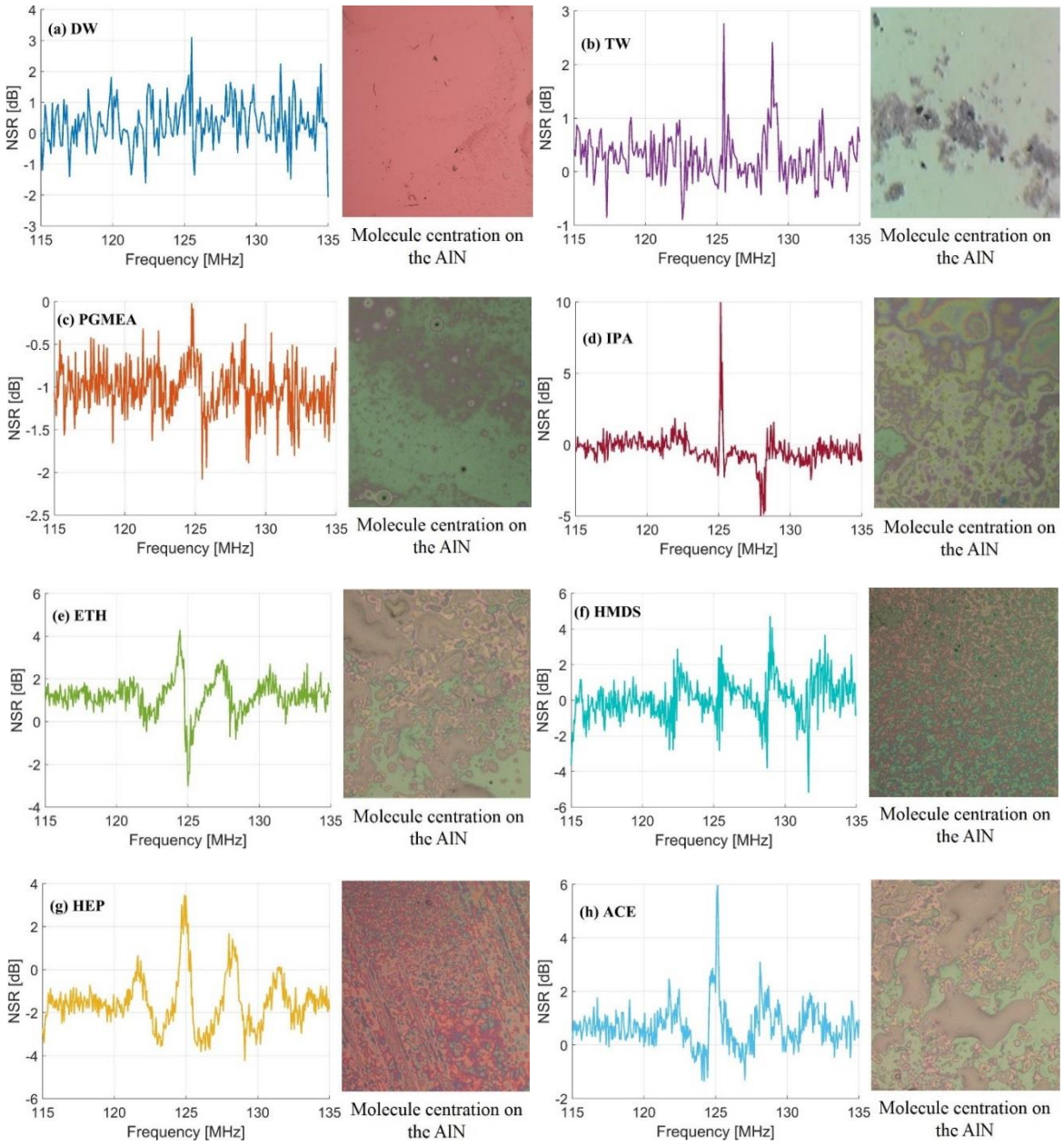

Fig. 8: Noise signal ratio (NSR) of the output signal before and after dropping the liquid for (a) DW, (b) TW, (c) PGMEA, (d) IPA, (e) ETH, (f) HMDS, (g) HEP and (h) ACE.

The presence of the stagnant liquid molecules leads to change in the mass density on the surface, thus making the output signal frequency shift and the noise increases as compared to the signal before dropping the liquid. Based on the uniform color of recorded micrographs, the form of PGMEA, TW, and DW molecules left are almost monolayer patterns, while that of others has almost multilayer patterns. The variation of the mass density is proportional to the increase of the stagnant liquid molecules on the surface. The generated noise-to-signal ratio (NSR) is shown in Fig. 8. Micrographs of the propagation path of the SAW device after the evaporation process of IPA, ACE, ETH, HMDS and HEP show rather concentrated latex molecules. Based on the interference patterns of the liquid meniscus, liquid molecules are packed inside varying multiple layers. Their noise signal

ratio oscillates more, especially at the center frequency. Therefore, like the order of the liquids as shown in Fig. 5b, the noise signal ratio (NSR) of DW, TW and PGMEA is the smallest and sparsest whereas the others have more oscillation at the center frequency, especially ACE because of the obstruction of the many layers of molecules and the higher molecule concentration.

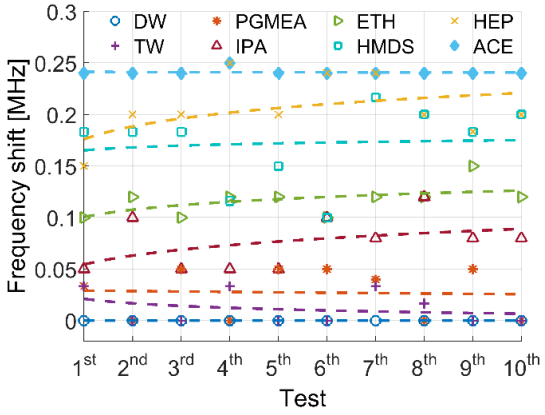

Fig. 9: Frequency shift of the SAW transducer for different liquids tested.

Table 3: CHARACTERISTICS OF EIGHT LIQUIDS IDENTIFIED BY THE SAW TRANSDUCER

Substance	***Physical property***				***Mass loading***			
	Slow attenuation		***No slow attenuation***		***Noise***		***Average frequency shift***	
	α_{MAX}	Duration of $\alpha > 0$	α_{MAX}	Duration of $\alpha > 0$	NSR < 5 dB	NSR > 5 dB	$\Delta f > 100\ kHz$	$\Delta f < 100\ kHz$
ACE			~ 14 dB	~ 20 s		x	241 ± 1	
HEP	~ 5 dB	50 s				x	206 ± 9.4	
HMDS	~ 6.6 dB	70 s				x	172 ± 11	
ETH			~ 5 dB	~ 20 s		x	117 ± 4.7	
IPA			~ 4 dB	~ 15 s		x		76 ± 8
PGMEA	~ 8 dB	160 s			x			27.3 ± 7.6
TW	~ 20 dB	200 s			x			11.6 ± 4.9
DW	~ 20 dB	250 s			x			0

As the frequency shift is proportional to the molecule concentration of the stagnant liquid on the propagation path, the order of the decreasing frequency shift of ACE, HEP, HMDS, ETH, IPA, PGMEA, TW and DW is in good agreement with the predicted one based on the theoretical analyses presented in section II.B. The frequency shift is calculated from the frequency difference of the attenuation peaks before and after the liquid evaporation process, and is shown in Fig. 9. If tap water is referred to a reference sample for noise caused by stagnant liquid molecules on the propagation path, a product (NS_i) of the molecule sensitivity factor and the stagnant liquid molecule, referred to a liquid sensitivity factor, is calculated by the measured frequency shift as shown in Eq. 9. Values of 20.66, 17.69, 14.71, 10.29, 6.51, 2.34 and 0 g/cm^2 are in regards to liquid sensitivity factors of ACE, HEP, HMDS, ETH, IPA, PGMEA and DW, respectively. It demonstrates a match of optical images (see Fig. 8) and experimental data (see Fig. 9) of eight liquids. For quite different samples like DW and IPA, it can be detected by a parameter like the presence of slow attenuation region of the fractional change, variation duration of the fractional change or noise. For

quite similar samples like ACE and IPA or DW and TW, the detection process needs more observations like deformation velocity of the contact area, noise and frequency shift. Table 3 summarizes the characteristics of the eight liquids tested, demonstrating that it is indeed possible to identify these liquids using the SAW transducer.

V. CONCLUSIONS

This paper presents a potential method for identifying liquid samples of microliter volumes in microfluidic biosensors. It is based on a surface-acoustic-mode AlN transducer using two detection mechanisms, physical properties and mass loading, during and after the evaporation process of the liquid. The fraction change of the attenuation is proportional to physical properties, such as evaporation rate, sound speed and density of the liquid. The frequency shift after the evaporation process is a function of the concentration of stagnant liquid molecules. The oscillation magnitude and duration of the fraction change α, noise-to-signal ratio *NSR* and frequency shift Δf are a good approach to recognize the type of liquid. The obtained experimental data for eight liquids, ACE, HEP, HMDS, ETH, IPA, PGMEA, TW and DW, are in good agreement with the theoretical analyses, thus validating the effectiveness of the proposed method.

VI. ACKNOWLEDGEMENTS

The authors would like to acknowledge the support of Dr. Henk van Zeijl and Tom Scholtes at EKL lab of the Delft University of Technology, Dr. An T. Tran at Advanced Institute for Science and Technology, Hanoi University of Science and Technology and Dr. Catalin V. Rusu from the Computer Science Department at Babes-Bolyai University.

This work is partly supported by a Vietnamese Government scholarship.

REFERENCES

[1] K.-Y. Hashimoto, M. Yamaguchi, Excitation and propagation of shear-horizontal-type surface and bulk acoustic waves. *Ultrasonics, Ferroelectrics, and Frequency Control, IEEE Transactions on* **48**, 1181-1188 (2001).

[2] J. Kondoh *et al.*, in *Frequency Control Symposium, 2007 Joint with the 21st European Frequency and Time Forum. IEEE International*. (2007), pp. 20-24.

[3] S. J. Martin, A. J. Ricco, T. M. Niemczyk, G. C. Frye, Characterization of SH acoustic plate mode liquid sensors. *Sensors and Actuators* **20**, 253-268 (1989).

[4] S. J. Martin, A. J. Ricco, G. C. Frye, T. M. Niemczyk, I. Adhihetty, in *Ultrasonics Symposium, 1988. Proceedings IEEE 1988*. (1988), pp. 607-611 vol. 601.

[5] S. Shiokawa, K. Jun, Surface Acoustic Wave Sensors. *Japanese Journal of Applied Physics* **43**, 2799 (2004).

[6] S. Shiokawa, Y. Matsui, T. Ueda, in *Ultrasonics Symposium, 1989. Proceedings, IEEE 1989*. (1989), pp. 643-646 vol. 641.

[7] G. Zhang, "Nanostructure-Enhanced Surface Acoustic Waves Biosensor and Its Computational Modeling", *Journal of Sensors*, vol. 2009, Article ID 215085.

[8] T. H. Bui, B. Morana, A. Tran, T. Scholtes, T. Chu Duc and Pasqualina M. Sarro, in *IEEE-SENSORS2015*. (Korea, 2015), pp. 323-327.

[9] B. T. Hang, D. Tung Bui, D. Trinh Chu, Microfluidic Injector Simulation with FSAW Sensor for 3-D Integration. *Instrumentation and Measurement, IEEE Transactions on* **64**, 849-856 (2015).

[10] B. T. Hang, D. Trinh Chu, in *SENSORS, 2013 IEEE*. (2013), pp. 1-4.

[11] P. Koštial, Surface acoustic wave measurements of evaporation rate. *Applied Acoustics* 47, 121-127 (1996).

[12] K. Länge, B. E. Rapp, M. Rapp, Surface acoustic wave biosensors: a review. *Analytical and Bioanalytical Chemistry* 391, 1509-1519 (2008).
[13] A. Prasad, A. T. H. Lin, V. R. Rao, and A. A. Seshia, "Monitoring sessile droplet evaporation on a micromechanical device," *Analyst*, vol. 139, pp. 5538-5546, 2014.
[14] J. Wei, P. M. Sarro, and C. D. Trinh, "A piezoresistive sensor for pressure monitoring at inkjet nozzle," in *Sensors, 2010 IEEE*, 2010, pp. 2093-2096.
[15] N. Blaz, A. Mari, S. Toskov, G. Miskovic, *et al.*, "Capacitive sensor for quantity detection of known liquid present in distilled water", *Proceedings of the 37th International Spring Seminar on Electronics Technology*, 2014, pp. 438-441.
[16] R. M. W. J. Ballantine, S.I. Martin, A.J. Ricco, E.T. Zellers, G.C. Frye and H. Wohltjen, *Acoustic Wave Sensors, 1st Edition: Theory, Design, & Physico-Chemical Applications*. (ACADEMIC PRESS, USA, 1997), pp. 56-100.
[17] S. Semenov, V. Starov, and R. G. Rubio, "Chapter 21 - Droplets with Surfactants A2 - Brutin, David," in *Droplet Wetting and Evaporation*, ed Oxford: Academic Press, 2015, pp. 315-337.
[18] M. Bishop, in *Introduction to Chemistry* (Prentice Hall, 2001).
[19] K. Dransfeld, E. Salzmann, in *Physical Acoustics*, W.P. Mason, R.N. Thurston Eds., (Academic press, New York, 1970) pp. 219-272.
[20] J. M. Stauber, S. K. Wilson, B. R. Duffy, K. Sefiane, On the lifetimes of evaporating droplets with related initial and receding contact angles. *Physics of Fluids* **27**, 122101 (2015).
[21] S. Dash and S. V. Garimella, "Droplet Evaporation Dynamics on a Superhydrophobic Surface with Negligible Hysteresis," *Langmuir*, vol. 29, pp. 10785-10795, 2013/08/27 2013.
[22] T. L. Berman, A. S. Lavine, F. P. Incropera, D. P. Dewitt, *Introduction to Heat Transfer*, John Wiley & Sons: New York, 7th ed., 2011.
[23] F. D. Lopez-Hilfiker, C. Mohr, E. L. D'Ambro, A. Lutz, T. P. Riedel, C. J. Gaston, *et al.*, "Molecular Composition and Volatility of Organic Aerosol in the Southeastern U.S.: Implications for IEPOX Derived SOA," *Environmental Science & Technology*, vol. 50, pp. 2200-2209, 2016/03/01 2016
[24] P. E. Liley, G. H. Thomson, D. G. Friend, T. E. Daubert, E. Buck, *Physical and Chemical Data*, The McGraw-Hill Company, 1999.
[25] G. Wyllie, Evaporation and Surface Structure of Liquids. *Proceedings of the Royal Society of London A: Mathematical, Physical and Engineering Sciences* **197**, 383-395 (1949).
[26] T. E. Parker, G. K. Montress, Precision surface-acoustic-wave (SAW) oscillators. *IEEE Transactions on Ultrasonics, Ferroelectrics, and Frequency Control* **35**, 342-364 (1988).
[27] Agilent, *Agilent Network Analyzer Basics*, report 2004.
[28] M. Bishop, in *Introduction to Chemistry* (Prentice Hall, 2001).
[29] B. S. Yaakov; L.X. Rong; K. Thiagalingam, *Estimation with Applications to Tracking and Navigation*, New York: John Wiley & Sons. pp. 308–317. ISBN 978-0-471-41655-5, 2001.